Reply to the comments of Reviewer No. 2

Levin Klein on behalf of the authors
IAG, University of Stuttgart

August 29, 2018

The authors would like to thank the reviewer for his/her efforts and constructive comments again. They are very much appreciated and incorporated into the revised manuscript.

In this document the comments given by the 2nd reviewer are addressed consecutively. The following formatting is chosen:

- The reviewer comments are marked in blue and italic.
- The reply by the authors is in black.
- A marked-up manuscript is added. Changed sections with regard to the comments by reviewer 2 are marked in orange.

General comments "C"

1. "*Paper length: I personally find the paper too long. It takes several hours to go through it and I had to read it multiple times to capture all the aspects. In my opinion the paper has several nice findings, which however currently do not emerge clearly. Several paragraphs look more from a technical report than from an actual scientific publication. A first example consists of the way the overall goal of the work is presented. This does not stand up in the text and it is only embedded in the text at page 3-line 3. This should to me be isolated in a well identified paragraph, so that readers (even quick readers) cannot miss it. A second example consists of paragraph 2.5.6 (with Figure 5). Does it improve readability to use almost one full page to discuss about numerical setups to decrease the CPU time? It has been certainly useful during the work, but I don't find this paragraph very useful. My suggestion is to shrink the overall paper, focusing on the strength of the computational setup and better highlighting the important findings about low-frequency emissions of WTs.*"
The authors splitted the section Introduction in several subsections to improve readability and to better highlight the aims of the paper, see **R2:C1-a** (page 1, line 20), **R2:C1-b** (page 2, line 44) and **R2:C1-c** (page 3, line 69).
The authors agree with the reviewer that the discussion about the numerical setup is not relevant for the understanding of the paper. They fully removed section 2.5.6 (Computational approach), see **R2:C1-e** (page 11, line 265).

2. "*Comparisons: The whole section 3 is also in my opinion too long, with the focus that is more biased towards unrealistic setups (Sect. 3.1) than the realistic ones (3.3). I would consider reducing the number of comparisons, focusing on maybe 3 cases: rigid-steady state inflow, elastic-steady state inflow, elastic-turbulent. I understand that the current structure of*

the paper aims at distinguishing each and every single phenomenon. However I see the risk of focusing on numerical artifacts more than on actual results and realistic phenomena."

The authors agree that some setups are relatively unrealistic. But a main task was to evaluate how the complexity of the setup changes the results. Many of the conclusions can not be drawn when numbers of setups is reduced. In CFD simulation it is often not possible to do a coupled simulation, because there is no structural model or even no fluid-structure coupling available. So it is quite important to see which effects can be captured without FSI and which not, and how big the difference might be.

3. *"Appearance The paper is generally well prepared and several nice plots help the understanding of the reader. However I suggest to eliminate some of the plots and enlarge others. Figure 1 is for example to me not needed, as well as all diagrams showing Fz and Mz. As expected, Fz and Mz never show anything interesting. Some other figures also don't add much to the discussion, see for instance Figure 10 as well as Figure 16. All plots containing the spectra could instead be enlarged to the full size of the page. Please be aware that when printed black/white all spectra are not easily readable."*

As suggested, the authors removed Figure 1 and 10 and the corresponding text from the paper. Figure 16 was also removed, but leaving the description of the results in the text.
To improve the readability and shorten the paper the authors removed F_z and M_z from the tower base load section as suggested. As F_x and M_y as well as F_y and M_x show very similar behaviour, the authors decided to focus on the bending moments M_x and M_y and removed the forces from the paper.
In the evaluation of the acoustic results observers A and B were removed from the figures as the behaviour of Observer C is very similar to observer A and the same applies to observers B and D. They are still mentioned in the text in connection with directivity to emphasize the similarity/symmetry.
Only a few adjustments had to be made in the text, most are just deletions (see **R2:C3-a** (page 5, line 140) to **R2:C3-aw** (page 24, line 473))
The remaining figures of tower base loads and observer spectra were enlarged to the width of on column in the final paper (before 6cm, now 8cm).

4. *"Present vs past tense: I personally prefer papers written in present tense, while this text mixes present and past tenses, sometimes in a conflicting fashion. This does not improve readability. Please review the text for consistency."*

The authors agree that the tenses are not consistent and revised the whole paper, switching past tense to present tense where reasonable, **R2:C4-a** (page 3, line 79) to **R2:C4-aj** (page 11, line 283).

Additional comments "AC"

1. *"Page 1 line 1: I would add "wind" before turbine "*

Added "wind" (**R2:AC1** (page 1, line 1)).

2. *"Page 1 line 8: I would reformulate the sentence "The tower base loads tend to be dominated by structural eigenfrequencies with increasing complexity of the model". The sentence is not clear, and when read alone is even fairly questionable."*

The authors reformulated the sentence, see **R2:AC2** (page 1, line 9).

3. *"Page 1 line 9: Although the whole paper is about low-frequency noise, I think it would not harm to add "low-frequency" before "aeroacoustic emissions""*

Added "low-frequency"(**R2:AC3** (page 1, line 11)).

4. *"Page 1 line 18: I'd anticipate the verb "occur" before "in a broad frequency range" "*

Changed it, see **R2:AC4** (page 1, line 22).

5. *"Page 1 line 19: check the "and" and the "," in the overall sentence formulations"*

R2:AC5 (page 1, line 23)

6. *"Page 2 line 5: "Hence" may be the wrong logical connector"*

Rewrote the previous sentence to make it clearer (**R2:AC6** (page 2, line 35)).

7. *"Page 2 line 8: The paragraph is not well connected to the previous one"*

Added a sentence for connection, see **R2:AC7** (page 2, line 39).

8. *"Page 2 line 30: Across the text you refer to other authors as "He" or "They". I'd prefer the passive forms for the verbs, but if you like it so, you should be consistent. Li et al. should be "They""*

Changed "he" and "his" to "they" and "their", see **R2:AC8** (page 3, line 65).

9. *"Page 2 line 33: "A totally new ..." may not be the right set of words to describe a coupling of existing tools within a scientific publication"*

Changed "new" to "revised" (**R2:AC9** (page 3, line 70)).

10. *"Page 3 line 11: What does "strong coupling" mean?"*

The authors removed "strong" (**R2:AC10** (page 3, line 84)), as, in their eyes, "strong coupling" is actually not clearly defined in literature. The authors originally wanted to describe "time accurate and two-way coupling" with "strong" which is described later on in more detail without using the word "strong".

11. *"Page 4 line 1: Tenses should all be reviewed, but here "SIMPACK is" should to me be replaced by "SIMPACK has been""*

Changed it, see **R2:AC11** (page 4, line 103).

12. *"Page 8 line 13: Nacelle hub are defined as rigid body, while foundation is a rigid body connected to the ground through a spring/damper system. However in table 2 (page 9) nacelle is listed among the flexible bodies and at page 10 line 8 it is written "flexible blades as well as a flexible tower and foundation". By "non-flexible foundation" does it mean that the degrees of freedom of the spring-damper are frozen? And what about nacelle? Please clarify."*

You are right, this is confusing. Removed "nacelle" from table as it is rigid and only moving with the flexible tower (Table 2 (page 10)). Yes, "non-flexible" means zero degrees of freedom.

13. *"Page 8 line 14: "Details" and not "Detail""*

Changed it, see **R2:AC13** (page 8, line 220).

14. *"Page 8 line 15: Here "was" is used, while a few lines later (page 9 line 2) the tense is back to present"*

The authors revised the whole section and switched the tense to present (**R2:AC14-a** (page 8, line 222) to **R2:AC14-e** (page 8, line 228)).

15. "*Page 11 line 10: In the low frequency domain the wave length is high and spectra cannot be accurately measured too close to the emitter. In the work 3600 observers are placed and the closest are only 100 m from tower base. Is the time history from those observers still accurate for the frequency band of interest? Please explain.*"

It is very likely that there are near field effects at a distance of 100m. That's why spectra at the observers at 1000m are regarded and the whole carpet of observers is only used to show the directivity and that 1000m is out of near field, see section 3.1.2 (page 14).

16. "*Page 10 line 12: Please evaluate the need to include paragraph 2.5.6*"

As stated above, the authors removed the whole paragraph from the paper.

17. "*Page 12: The case LC1 is without tower and nacelle. How and where are the loads computed? Even though there is uniform inflow and no tower, shouldn't you see some periodicity in the signal due to the tilt angle?*"

As stated in the text, only aerodynamic loads, calculated with respect to the tower base coordinate system, are compared. Added "(moment reference point)" for better understanding **R2:AC17-a** (page 13, line 295) and adopted caption of Figure 6 (page 13). At blade passing frequency there actually is a small peak in F_x and M_y and a more prominent one for M_z. Obviously the impact on M_x, F_y and F_z is very low.

18. "*Page 13 line 8: Please better explain the sentence "Therefore, aerodynamic loads on rotor and tower were evaluated separately." How exactly? Always at tower base?*"

Aerodynamics loads from CFD simulations are obtained from integration over surfaces as described in paragraph 2.3.3 (page 5). This has just been done separately for the surfaces of the rotor and the tower. Adopted the text and caption of figure for better understanding (**R2:AC18-a** (page 14, line 306), **R2:AC18-b** (page 14, line 307) and Figure 7 (page 15)).

19. "*Page 13: In figure 8, I understand the general increase of amplitudes below BPF due to shedding on the tower. Fx and My have an increase of amplitudes on the band between 5-9 Hz for LC1 and LC2. For Mz this is even more noticeable. This behavior does not appear in LC2_FSC1SD. Could you please explain what happens?*"

Removed Diagram with M_z from Figure as suggested by reviewer. In M_y increased amplitudes at 5-9Hz are on a very low level ($\approx 0.2\%$ of maximum amplitude in case LC2).

20. "*Page 14: My guess is that a Strouhal number of 0.2 was chosen as it is typical for cylinders, but it isn't mentioned. Rotor is operating at rated conditions, so let's suppose an axial induction factor of 0.33, this means that the tower experiences a flow speed of 11.3*(1-0.333)= 8 m/s. Considering the asymptotic wind speed and the average diameter, a Reynolds number around 2e6 can be calculated. Is 0.2 still a typical Strouhal number even at such Reynolds number? Please discuss.*"

The authors adjusted the Strouhal number to 0.24 which better fits the high Reynolds number. Adopted the text accordingly (**R2:AC20** (page 14, line 315)).

21. "*Page 14: 0.292 Hz should be the frequency where vortex shedding occurs. However, I don't clearly see a precise peak at this frequency. What I notice is that AROUND this frequency range there is a general increase in side-side Fy and Mx amplitudes, which makes sense because shedding frequency varies along the tower because of different diameter and inflow. Do I understand things right?*"

Yes, that's how the authors understand it too. As the highest peak in this frequency range is at 0.292 Hz it was chosen for the evaluation of surface pressure. For sure there is a general increase in the frequency range around this frequency. Adopted text for better understanding, see $\boxed{\textbf{R2:AC21}}$ (page 14, line 321).

22. "*Page 24 line 30: "generic" or "conceptual" wind turbine?*"

"Generic" is widely used in the context of the NREL 5MW turbine which is the basis of the investigated turbine.

23. "*Page 25 line 30: In my opinion stating that results are of "high quality" requires first a validation.*"

The capability of the CFD code for wind turbine simulations has been proven in several projects. E.g the European Avatar Project. A validation in the actual case is actually not possible. Nevertheless, the authors removed the whole sentence from the paper, ($\boxed{\textbf{R2:AC23}}$ (page 25, line 518)).

Advanced CFD-MBS coupling to assess low-frequency emissions from wind turbines

Levin Klein[1], Jonas Gude[1], Florian Wenz[1], Thorsten Lutz[1], and Ewald Krämer[1]

[1]Institute of Aerodynamics and Gas Dynamics, University of Stuttgart, Pfaffenwaldring 21, 70569 Stuttgart, Germany

Correspondence: Levin Klein (levin.klein@iag.uni-stuttgart.de)

Abstract. The low-frequency emissions from a generic 5 MW **R2:AC1** wind turbine are investigated numerically. In order to regard airborne noise and structure-borne noise simultaneously a process chain was developed. It considers fluid-structure coupling (FSC) of a computational fluid dynamics (CFD) solver and multibody simulations (MBS) solver as well as a Ffowcs Williams-Hawkings (FW-H) acoustic solver. The approach was applied to a generic 5 MW turbine to get more insight into the sources and mechanisms of low-frequency emissions from wind turbines. For this purpose simulations with increasing complexity in terms of considered components in the CFD model, degrees of freedom in the structural model and inflow in the CFD model were conducted. Consistent with literature, it has been found that aeroacoustic low-frequency emission is dominated by the blade-passing frequency harmonics. ~~The tower base loads, which excite seismic emission, tend to be dominated by structural eigenfrequencies with increasing complexity of the model. The~~ **R2:AC2** In the spectra of the tower base loads, which excite seismic emission, the structural eigenfrequencies become more prominent with increasing complexity of the model. The main source of **R2:AC3** low-frequency aeroacoustic emissions is the blade-tower interaction and the contribution of the tower as an acoustic emitter is stronger than the contribution of the rotor. Aerodynamic tower loads also significantly contribute to the external excitation acting on the structure of the wind turbine.

1 Introduction

Renewable sources of energy and especially wind power have seen a strong expansion in the last years. Even though the construction of large offshore wind farms is currently a strong focus, the potential of onshore wind turbines by opening up new, previously unused areas and repowering of existing sites is still significant. With regard to the acceptance and the fulfillment of stricter legal requirements concerning noise and vibrations, the research on low-frequency emissions from wind turbines gains importance.

1.1 **R2:C1-a** Emissions from wind turbines

As wind turbines are counted among the tallest machines on the planet that work in an uncontrolled outside environment, noise and vibration emissions **R2:AC4** occur in a broad frequency range~~occur~~. While sources of acoustic wind turbine emission in the audible range are widely researched~~,~~ **R2:AC5** and understood and different methods are applied to reduce aerodynamic and mechanical noise (Liu, 2017), there is much less known about low-frequency emissions from wind turbines. Many publications about low-frequency emissions ~~of~~ **Authors** from wind turbines concentrate on the impact on seismic measurements. The emitted ground motion signals from wind turbines are measured by local seismic stations built for detection of events with small magnitudes like far away earthquakes or nuclear weapons tests. Zieger and Ritter (2018) observed an increase of amplitudes in a frequency range from $0.5\,\mathrm{Hz}$ to $10\,\mathrm{Hz}$ dependent of the rotational speed of the turbine and thus wind speed at a distance of $5.5\,\mathrm{km}$ away from a wind turbine. This confirms the measurements by Stammler and Ceranna (2016) and Styles et al. (2005) who found that nearby wind turbines reduce the sensitivity of seismic stations as they introduce wind dependence into the measured noise spectra.

Acoustic measurements in the low-frequency range $3.3\,\mathrm{km}$ from a wind farm show discrete peaks at the blade-passing frequency (BPF) and its higher harmonics below $20\,\mathrm{Hz}$ (Hansen et al., 2017). This was also observed by Pilger and Ceranna (2017) who evaluated the data obtained by a microbarometer array for infrasound detection located in northern Germany. Zajamšek et al. (2016)~~investigated the measurability of these acoustic waves in buildings.~~ **R2:AC6** compared outdoor and indoor measurements close to an Australian wind farm and found the same tonal character in the noise spectra. Hence, the blade-tower interaction is seen to be responsible for aeroacoustic low-frequency noise of ~~windfarms~~ **Authors** wind farms (Van den Berg, 2005).

R2:AC7 The scope of research on low-frequency noise from wind turbines is often its impact on human beings. Knopper et al. (2014) conclude from their literature survey that human health is not likely to be affected by low-frequency noise and infrasound from wind turbines.Turnbull et al. (2012) state that the measured level of infrasound within two Australian wind farms was similar to that measured in urban and coastal areas and near other engineered noise sources.

1.2 **R2:C1-b** Numerical approaches on low frequency noise

For an optimization of the structure and foundations of future wind turbines as well as for the assessment of the impact of low-frequency noise and low-frequency seismic vibrations on the environment, reliable methods for the prediction of emissions are of great importance. Gortsas et al. (2017) performed a numerical study to calculate wave propagation using the Boundary Element Method. They developed a model which considers the mentioned seismic vibrations as well as the low-frequency noise in air and even allows a prediction of the sound pressure level (SPL) inside a generic building. But, as this model is only capable to calculate the propagation, reliable input data representing the airborne and structure-borne emissions from the wind turbine has to be provided. CFD simulations including fluid-structure interaction (FSI) are capable of providing both. Thus, Gortsas et al. used data made available by the authors of the present paper.

There are few studies on the modelling of aeroacoustic low-frequency emission from wind turbines. In the 1980s the NASA developed a code for predicting low-frequency wind turbine noise based on Lowson's acoustic equation applied on rotor forces (Viterna, 1981). Madsen (2010) presented a Blade Element Momentum (BEM) based investigation of low-frequency noise that uses the same theory for the aeroacoustic model. CFD simulations combined with the FW-H propagation method have been applied by Ghasemian and Nejat (2015) and Bozorgi et al. (2018) to assess low-frequency noise of wind turbine rotors. While Madsen considers the influence of the tower on the rotor aerodynamics, Ghasemian and Nejat and Bozorgi et al. study the isolated rotor. Yauwenas et al. (2017) investigated the blade-passage noise of a generic model turbine numerically using CFD and Curle's acoustic analogy. They found a significant contribution of the induced pressure fluctuations on the tower to the tonal blade-passage noise which was validated with experimental measurements.

In recent years, CFD based fluid-structure coupling has been applied frequently for the investigation of wind turbines. Li et al. (2017) presented a framework of a wind turbine aero-servo-elastic simulation including flexible blades and tower which allows motion of all turbine components. ~~In his approach, controllers for torque and blade pitch are included as well and he focuses his studies on the impact of FSI on aerodynamic rotor loads, drive train dynamics, controllers and wake.~~ **R2:AC8** In their approach, controllers for torque and blade pitch are included as well and they focus their studies on the impact of FSI on aerodynamic rotor loads, drive train dynamics, controllers and wake. Streiner et al. (2008) developed a coupling of the CFD code *FLOWer* to the multibody solver (MBS) *SIMPACK* with the capability to couple isolated wind turbine rotors.

1.3 **R2:C1-c** Scope and objectives

A totally ~~new~~ **R2:AC9** revised *FLOWer-SIMPACK* coupling is revealed in the present paper with the potential to take into account more degrees of freedom, like tower deformation or changes in rotational speed in the structural model and their impact on aerodynamics and aeroacoustics, respectively. Together with the already existing process chain, fully coupled CFD simulations under realistic turbulent inflow conditions can be conducted, providing both airborne and structure-borne emissions simultaneously. A FW-H in-house code is applied to calculate aeroacoustic immission at distant observers while tower base loads represent the structure-borne emission. The aim of the present paper is to identify the sources of low-frequency emissions and to investigate the impact of the complexity of the numerical model on the calculated low-frequency emissions from a generic $5\,\mathrm{MW}$ wind turbine. The complexity of the model ~~was~~ **R2:C4** is increased from a rotor only simulation with uniform inflow to a coupled simulation including blade, tower and foundation dynamics with turbulent atmospheric boundary layer. The spectra of tower base loads and acoustic immissions for overall 7 cases ~~were~~ **R2:C4-a** are compared in a frequency range from 0.1 to $25\,\mathrm{Hz}$ for evaluation.

2 Numerical process chain

A high fidelity process chain based on multiple solvers was established for the investigation of low-frequency emissions from wind turbines. It consists of the CFD solver *FLOWer*, the MBS solver *SIMPACK* and the FW-H solver *ACCO*. A ~~strong~~ **R2:AC10** coupling between *FLOWer* and *SIMPACK* was developed to generate high fidelity time series of surface pressure distribution on the turbine and structural loads (forces and moments) acting on the foundation of the turbine. Using the CFD results, the aeroacoustic signal at distant, predefined observer positions is computed by means of *ACCO*.

2.1 CFD solver

FLOWer is a compressible, dual time stepping, block structured Reynolds-averaged Navier-Stokes (RANS) solver developed by German Aerospace Center (DLR) (Kroll et al., 2000). The usage of independent grids for bodies and background is enabled by the overlapping grid technique *CHIMERA*, one of *FLOWers* main features. The solver is continuously extended at Institute of Aerodynamic and Gas Dynamics (IAG) regarding functionality and performance, including, amongst others, the higher order finite difference weighted essentially non-oscillatory (WENO) scheme (Kowarsch et al., 2013), Dirichlet boundary condition to apply arbitrary unsteady inflow, a body forces approach to superimpose turbulence (Schulz et al., 2016b) and various DES schemes (Weihing et al., 2016). The capability of *FLOWer* for wind turbine simulations has been shown in several projects. The interaction of a wind turbine in complex terrain with atmospheric turbulence was investigated by Schulz et al. (2016a) and code to code comparisons were recently conducted in the European *AVATAR* project (Schepers et al., 2016).

2.2 Multibody solver

SIMPACK is a commercial non-linear MBS solver that can be applied to simulate dynamic systems consisting of rigid and flexible bodies. Flexible turbine components like tower and blades are modeled with linear or nonlinear beam theory. The kinematics between the components are defined by joint elements and internal forces can be considered. There are two ways to apply external forces such as aerodynamic forces, either by built-in interfaces or by programmable user routines. Controllers can also be integrated. *SIMPACK* ~~is~~ **R2:AC11** has been recently applied by industry and research groups for the simulation of wind turbines, examples can be found in (Luhmann et al., 2017; Jassmann et al., 2014).

2.3 Fluid-structure interaction

To take the influence of unsteady structural deformation on the aerodynamics into account, a coupling between *FLOWer* and *SIMPACK* was implemented. The new approach generally allows coupling of slender beam like structures and is not limited to rotor blades or even wind turbines. Combined coupling of rotating and non-rotating parts can be applied and the deformation of adjacent structures is considered. Furthermore, coupling is not restricted to flexible deformations but also rigid body motions (rotations and translations) can be realized. In the application of wind turbines e.g. pitch motions and changes in rotational speed of the rotor can be transferred from the MBS solver to the CFD solver.

For the technical realization, an existing interface that was developed to couple *SIMPACK* with the fluid solver *ANSYS CFX* for the investigation of a tidal current turbine (Arnold et al., 2013) was extended. Furthermore, libraries for grid deformation and load integration which were recently developed and integrated into *FLOWer* (Schuff et al., 2014; Kranzinger et al., 2016) had to be extended for the coupling with *SIMPACK*. Besides the functionality, the main target of the implementation was to keep the set-up of the coupling simple and the dependencies between MBS and CFD models low. Thus, resolution of CFD and MBS model are independent of each other which allows a fast and easy adjustment and replacement of MBS structures or CFD meshes. Furthermore, the new coupling can be restarted, allowing much longer simulation times if *FLOWer* runs on clusters with limited job duration. It was already successfully applied on the blade of a generic $10MW$ turbine for comparison reasons by Sayed et al. (2016) who implemented a coupling of *FLOWer* to the structural dynamics solver *Carat++*.

2.3.1 General functionality

The developed coupling is a partitioned approach, where two independent solvers run simultaneously on different machines and exchange data via Secure Shell (SSH) connection at discrete positions, so called markers. The markers are positioned inside the bodies. While rigid bodies have only one marker, flexible bodies like rotor blades have several markers that are distributed along the beam. On the one hand, deflections and rotations of these markers relative to their non-deformed position are computed by *SIMPACK*. On the other hand, aerodynamic forces and moments acting on these markers are calculated in *FLOWer*. For each structure that is coupled, a communication coordinate system is defined that has to be in the same position and same orientation in both models at all times. It does not have to be fixed, but can be rotating or translating in a predefined way. All data concerning the respective structure is communicated in this coordinate system.

2.3.2 Mesh deformation

The task of the deformation library implemented in *FLOWer* is to apply the deformations of the markers on the corresponding CFD surfaces and to deform the surrounding volume mesh accordingly. The surface is represented by a point cloud which is generated from the CFD mesh. For rigid structures only one marker is used and all surface cloud points perform a rigid body motion based on the translation and rotation of this marker. A cubic spline interpolation is applied for the mapping of flexible structures (beams) consisting of more than one marker. The deformation of each surface cloud point is then realized as rigid body motion based on the corresponding positions along the beam. While a complete spline approach is used for the deflections, taking the rotation at the end points into account, the rotations and the non-deformed marker positions are interpolated using natural splines. A similar approach has been presented by Arnold et al. (2013). ~~Figure 1 shows the surface grid deformation for the first bending mode in a simple test case with 3 markers. Spline interpolation gives a much smoother result in comparison to linear interpolation and considers the non-rotated lower end.~~ **R2:C3-a** Finally, the volume grids are deformed based on the deformation of the point cloud using radial basis functions. To ensure correct overlapping of deformed meshes, holes associated to the deformed surface can also be deformed.

~~Figure 1: Undeformed (black) and deformed (grey) surface mesh, linear interpolation (left) and spline interpolation (right) for a simple test case with three markers. Generic deformation of first bending mode. Rotation at lower end is zero.~~ **R2:C3-b**

2.3.3 Load integration

The load library implemented in *FLOWer* enables the calculation of aerodynamic loads on grid surfaces by integration of friction and pressure over the cell faces.~~For the coupling to *SIMPACK*, the CFD surface is divided into segments based on the deformed marker positions. Loads are integrated for these segments and assigned to the respective markers.~~ **R1:Mi2** This is also necessary for the coupling to *SIMPACK*, as there is no surface in the structural model and the aerodynamic forces have to be mapped to the discrete marker positions. For this purpose, the CFD surface is divided into segments based on the deformed marker positions. For each of these segments, loads are integrated and afterwards assigned to the respective markers. Moments

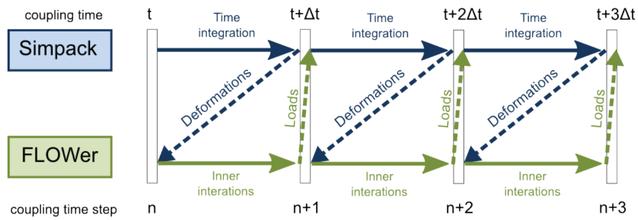

Figure 1. Explicit coupling scheme of the *FLOWer-SIMPACK* coupling.

are calculated with respect to the origin of the corresponding communication coordinate system. For structures with only one marker, loads are integrated over the whole CFD surface of the respective structure.

2.3.4 Communication interface

The communication is realized by means of files. Data files contain deformations or loads and status files indicate that the data file is ready to be read. While *SIMPACK* is running on a local Windows machine, *FLOWer* is usually executed in parallel mode on a high performance computing (HPC) system running on Linux. A portable communication script in Windows inherent scripting language PowerShell enables fast and reliable communication between the two solvers. The Linux machine is accessed using a SSH connection via the Windows Secure Copy (WinSCP) client.

2.3.5 Coupling scheme

In the presented work, an explicit coupling scheme ~~was~~ **R2:C4-b** is applied. The size of the coupling time step is equal to the physical *FLOWer* time step and remains constant throughout the simulation. Both solvers are running in a sequential way, waiting for the other solver to reach the next time step and to send communication data. *SIMPACK* is running one time step ahead doing time integration with the aerodynamic loads that *FLOWer* computed at the end of the previous time step (Figure 1).

2.4 Acoustic solver

Acoustic immission at arbitrary observer locations ~~was~~ **R2:C4-c** is calculated by means of the in-house FW-H solver *ACCO*. Pressure and velocities on surfaces enclosing the noise sources are evaluated at each time step of the transient CFD solution, including velocities due to deformation, translation and rotation. For the present study, the surfaces used for the acoustic analysis ~~were~~ **R2:C4-d** are identical with the physical surfaces of the turbine (rotor, tower, hub etc.). Volume sources generated by free-flow turbulence ~~were~~ **R2:C4-e** are neglected, which is justified for low mach number flow because quadrupole volume noise is proportional to Ma^7. This approach was validated for a rod-cylinder configuration and an airfoil in turbulent flow (Lutz et al., 2015; Illg et al., 2015). The acoustic monopole and dipole contributions to the observer sound pressure level (SPL) are computed by means of the Ffowcs Williams-Hawkings (FW-H) equation. Its left-hand side is the wave equation which describes the transmission of sound to the observer, presuming undisturbed propagation and observers located in the acoustic far field. Hence, ground reflections and non-linear propagation due to atmospheric layering and turbulence are not taken into account. The acoustic far field is defined by the presence of a fully developed wave front and thus starts several wave lengths away from the source. Parallel execution of *ACCO* allows the computation of noise carpets consisting of several thousand observer locations.

The application of the FW-H analogy allows evaluation of the contribution of selected components of the wind turbine to SPL by excluding surfaces of particular components (e.g. tower) from the analysis.

2.5 Computational set-up

2.5.1 The turbine

The examined turbine is based on the NREL $5\,\mathrm{MW}$ turbine (Jonkman et al., 2009) and was slightly modified in the *OFFWINDTECH* project (Bekiropoulos et al., 2013). The main modifications concern the rated conditions which were changed to a rotational speed of $11.7\,\mathrm{RPM}$ and a pitch angle of $-2.29°$ at a wind speed at hub height of $11.3\,\mathrm{ms}^{-1}$. The turbine ~~was~~ **R2:C4-f** is investigated at rated conditions in an onshore configuration with a hub height of $90\,\mathrm{m}$, a rotor diameter of $126\,\mathrm{m}$ with a tilt angle of $5°$ and a precone angle of $2.5°$. The original tower with a bottom diameter of $6\,\mathrm{m}$ and a top diameter of $3.87\,\mathrm{m}$ ~~was~~ **R2:C4-g** is used.

2.5.2 CFD model

The CFD model of the *OFFWINDTECH* turbine consists of ten independent body meshes, that are embedded in a Cartesian hanging grid node background mesh using the *CHIMERA* technique. Blades, hub, nacelle and tower ~~were~~ **R2:C4-h** are considered in the simulation with fully resolved boundary layer ($y^+ \leq 1$). No gaps are left between the components of the turbine, as blade-hub connectors and a hub-nacelle connector are included in the CFD mesh (Figure 2). Blades ~~were~~ **R2:C4-i** are meshed in a C-H-mesh topology with 120 cells in radial direction and 180 cells around the airfoil, summing up to approximately 5.3 million cells per blade. Two different Cartesian background grids ~~were created using hanging grid nodes~~ **R2:C4-j** with hanging grid nodes are used. One for the case with prescribed atmospheric turbulence where the mesh is additionally refined to a cell size of $1\,\mathrm{m}^3$ upstream of the turbine (64.5 million cells) and another for the case without atmospheric turbulence where only the mesh close to the turbine is refined (20.8 million cells). The computational domain is approximately 48.8 rotor radii (R) long ($12.7\,R$ upstream of the rotor plane), approximately $24.4\,R$ wide and has a height of approximately $16.2R$. According to a previous study using *FLOWer* (Sayed et al., 2015), the background grids ~~were expanded~~ **R2:C4-k** expand more than sufficient in all directions to avoid influence on the flow field around the turbine. Overall the two set-ups consist of 86 million (fine) respectively 42 million cells (coarse).

Concerning inflow three different cases are regarded in the present study. Uniform inflow, steady atmospheric boundary layer and turbulent atmospheric boundary layer. An exponent of 0.19 ~~was~~ **R2:C4-l** is applied for the power law profile describing the steady atmospheric boundary layer, keeping the wind speed at hub height at $11.3\,\mathrm{ms}^{-1}$. Atmospheric turbulence with a reference length scale of $42\,\mathrm{m}$ ~~was created using~~ **R2:C4-m** , created using Mann's model (Mann, 1994) ~~and~~ **R2:C4-n** , is

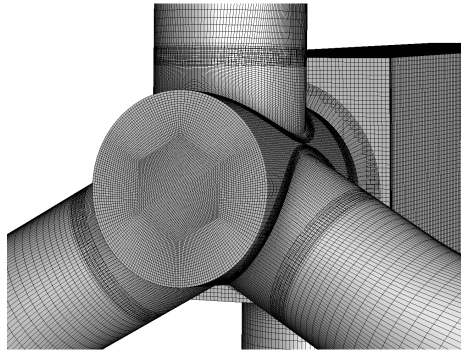

Figure 2. CFD surface mesh, showing the connection of hub, blades and nacelle with overlapping meshes.

introduced into the flow field using body forces $16\,\mathrm{m}$ downstream of the inlet, superimposing the steady boundary layer profile. The resulting turbulence level at the turbine position ~~was~~ **R2:C4-o** is 16%. Unsteady RANS (URANS) simulations ~~were~~ **R2:C4-p** are applied with a second order dual time stepping scheme for temporal discretisation. The second order central discretisation with the Jameson-Schmidt-Turkel (JST) artificial dissipation term ~~was~~ **R2:C4-q** is used for spatial discretisation in body meshes and fifth order WENO scheme ~~was~~ **R2:C4-r** is applied on the background mesh in order to reduce dissipation of vortices. Menter-SST (Menter, 1994) was deployed for turbulence modelling. A physical time step corresponding to $0.75°$ azimuth ~~($\approx 0.0168\,\mathrm{s}$)~~ **Authors** ($\approx 0.01068\,\mathrm{s}$) with 100 inner iterations ~~was~~ **R2:C4-s** is applied for the evaluated part of the simulations.

2.5.3 Structural model

The *SIMPACK* model of the *OFFWINDTECH* turbine was built by Matha et al. (2010). The blades are modelled non-linear by using multiple flexible bodies per blade. The structural properties of the tower are adopted from the NREL $5\,\mathrm{MW}$ turbine (Jonkman et al., 2009) taking 20 modes into account. Hub and nacelle are defined as rigid bodies. The foundation is modelled as rigid body connected to the ground with a spring-damper system. ~~Detail~~ **R2:AC13** Details can be found in Table 1.

2.5.4 FSI setup

~~The coupling between *FLOWer* and *SIMPACK* for the *OFFWINDTECH* turbine was applied using 160 markers~~ **R2:AC14-a** 160 markers are used for the fluid structure coupling of the *OFFWINDTECH* turbine (Figure 3), 49 markers for each blade, 11 markers for the tower, and nacelle and hub with one marker each. Since in the structural model and the CFD model a fixed rotational speed ~~was~~ **R2:AC14-b** is prescribed, a rotating communication coordinate system in the center of the hub ~~was~~ **R2:AC14-c** is used for the rotating parts. The communication for tower and nacelle ~~was~~ **R2:AC14-d** is performed in a fixed coordinate system placed at the tower base (Figure 3). In the *SIMPACK* model of the turbine, additional rigid bodies ~~were~~ **R2:AC14-e** are created for the definition of the undeformed markers. The corresponding moving markers ~~were~~ **R2:AC4-f** are attached to the flexible structures of the turbine. With this approach the measured deformations between deformed and

Table 1. Details on the foundation of the wind turbine, similar to Gortsas et al. (2017).

Mass	$1.888e6\,\mathrm{kg}$
Inertia x, y	$82.705e6\,\mathrm{kgm}^2$
Inertia z	$88.529e6\,\mathrm{kgm}^2$
Stiffness x, y	$8.554e9\,\mathrm{Nm}^{-1}$
Stiffness z	$7.332e9\,\mathrm{Nm}^{-1}$
Rotational stiffness x, y	$559e9\,\mathrm{Nm} \cdot \mathrm{rad}^{-1}$
Rotational stiffness z	$559e9\,\mathrm{Nm} \cdot \mathrm{rad}^{-1}$
Damping x, y	$240e6\,\mathrm{Nsm}^{-1}$
Damping z	$325e6\,\mathrm{Nsm}^{-1}$
Rotational damping x, y	$5.035e9\,\mathrm{Nms} \cdot \mathrm{rad}^{-1}$
Rotational damping z	$4.180e9\,\mathrm{Nms} \cdot \mathrm{rad}^{-1}$

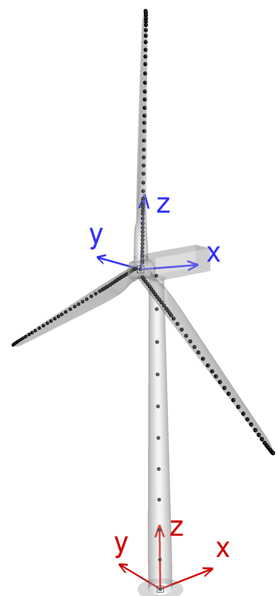

Figure 3. CFD surface of turbine including markers for coupling with *SIMPACK*. Rotating hub coordinate system is shown in blue and tower base coordinate system in red.

undeformed markers are composed of flexible deformations of the body itself plus rigid body motion due to deformation or motion of the adjacent body.

Table 2. Definition of simulation cases, ordered with increasing complexity.

Case name	Inflow	CFD structures	Flexible structures	Background mesh
LC1	uniform	rotor	none	coarse
LC2	uniform	rotor, nacelle, tower	none	coarse
LC2_FSC1SD	uniform	rotor, nacelle, tower	rotor blades SD	coarse
LC2_FSC1	uniform	rotor, nacelle, tower	rotor blades	coarse
LC2_FSC3	uniform	rotor, nacelle, tower	~~rotor, nacelle,~~ **R2:AC12-a** rotor blades, tower, foundation	coarse
LC3_FSC3	steady ABL	rotor, nacelle, tower	~~rotor, nacelle,~~ **R2:AC12-b** rotor blades, tower, foundation	fine
LC4_FSC3	turbulent ABL	rotor, nacelle, tower	~~rotor, nacelle,~~ **R2:AC12-c** rotor blades, tower, foundation	fine

ABL, atmospheric boundary layer; SD, steady deformation.

2.5.5 Simulation cases

In Table 2 all regarded simulation cases are listed. ~~Three studies were conducted~~ **Authors** For evaluation they are assigned to three studies. In the first study, no FSI ~~was~~ **R2:C4-t** is considered and thus all turbine components ~~were~~ **R2:C4-u** are kept rigid. The influences of the presence of the tower and the distance of the blade to the tower ~~were~~ **R2:C4-v** are evaluated at uniform inflow conditions by comparing LC1, LC2 and LC2_FSC1SD. In case LC2_FSC1SD the ~~averaged blade deformations of case LC2_FSC1 were used to create~~ **Authors** blade deformation is equal to the averaged blade deformation of case LC2_FSC1 to obtain a realistically deformed shape of the blades with reduced distance between blades and tower. In a second study the degrees of freedom of the structural model ~~were~~ **R2:C4-w** are increased at uniform inflow conditions. Three cases ~~were~~ **R2:C4-x** are compared: a rigid case with steady deformed blades (LC2_FSC1SD), a case with flexible blades (LC2_FSC1) and a case with flexible blades as well as a flexible tower and foundation (LC2_FSC3). In the third study, the inflow conditions ~~were changed~~ **R2:C4-y** are **Authors** varied, keeping the structural model the same. Case LC2_FSC3 is used as reference. A steady atmospheric boundary layer (ABL) ~~was~~ **R2:C4-z** is prescribed at the inlet by means of a power law inflow profile in case LC3_FSC3. This steady ABL ~~was~~ **R2:C4-aa** is superposed with velocity fluctuations modelling a turbulent atmospheric boundary layer in case LC4_FSC3.

2.5.6 ~~Computational approach~~

~~One feature of the implemented coupling is that coupled simulations can be started from results of standalone CFD simulations. This was applied in the presented research to achieve a well converged state concerning aerodynamic forces and flow field. At the same time computational costs could be saved, as coupled simulations with various degrees of freedom could be started from the same converged state. In all cases at least 32 revolutions were simulated before the start of the coupling. This was necessary due to the high induction of the rotor. The structural simulation is started from a initialized state at the beginning of the coupling. All flexible components are released from a rigid state and due to the sudden impact of gravitational, centrifugal~~

~~and aerodynamic forces, deformations tend to overshoot. As the CFD part of the coupled simulations is computationally expensive, it is important to have a fast convergence of deformations and loads to a periodic state. While flap-wise deflections of the blades are damped very fast, blade edge-wise deflections and tower deflections are not. *SIMPACK* allows the user to define time depended functions for external forces and dampers. As a first step, to reduce deformation velocity at the start of the coupling, aerodynamic loads are multiplied with a linearly increasing load factor over the first 120 time steps ($\approx 1,71\,\mathrm{s}$). Additionally, dampers in form of counter acting forces proportional to deformation velocity are attached to the tower tip as well as to the blades to damp initial oscillations of blades and tower. The damping factors are linearly increased and decreased over time and were determined manually for optimal performance of the model. Figure **??** exemplarily shows the force of the tower tip damper in x-direction and the deflection of the tower tip for case LC2_FSC3. The tower damping factor decreases to zero after 740 time steps ($\approx 7.91\,\mathrm{s}$). The tower tip deflection shows only a small overshoot and is well converged when the damper is switched off. With this approach, a fast convergence of deflections and loads was achieved and only the first two coupled revolutions of the turbine could not be used for evaluation.~~ **R2:C1-e**

2.6 Evaluation

The aim of the simulation chain is to model airborne and structure-borne emissions simultaneously by evaluating acoustic immission at distant observers and load fluctuations at the tower base. In the fluid-structure coupled simulations tower base loads ~~were~~ **R2:C4-ab** are evaluated directly in the structural model at the interface between tower and foundation, whereas in the non-coupled simulations aerodynamic loads ~~were~~ **R2:C4-ac** are computed from CFD results. In both cases the tower base loads are presented with respect to the tower base coordinate system which is shown in Figure 3. The temporal resolution of the data is equal to the coupling time step. To achieve the same temporal resolution in the acoustic emission, each time step a CFD surface solution ~~was~~ **R2:C4-ad** is saved **R1:Mi5-b** temporally as input for the acoustic simulations.
Acoustic simulations using *ACCO* ~~were~~ **R2:C4-ae** are conducted to calculate the immission at a carpet of observers on the ground surrounding the turbine. Figure 4 shows the 3600 observers located on 20 concentric rings around the turbine at radial positions of $100\,\mathrm{m}$ to $2000\,\mathrm{m}$ with a radial resolution of $100\,\mathrm{m}$ and a circumferential resolution of $2°$. Unweighted SPL ~~was~~ **R2:C4-af** is calculated from sound pressure time series at the observers with a reference sound pressure of $20\,\mathrm{\mu Pa}$. The sound propagation and directivity for discrete frequencies can be evaluated by plotting the SPL contour on the ground. Four observers at a distance of $1000\,\mathrm{m}$ to the turbine ~~were~~ **R2:C4-ag** are chosen for detailed evaluation of SPL spectra (large dots in Figure 4). Prior to frequency analyses by means of fast Fourier transform (FFT), the time series signals of loads and sound pressure ~~were~~ **R2:C4-ah** are cut to multiples of one rotational period of the turbine in order to supply a preferably periodical signal to the FFT and to avoid influence of start-up effects. In coupled simulations, the first two revolutions ~~were~~ **R2:C4-ai** are excluded from evaluation. For case LC4_FSC3 14 revolutions and for all other cases 8 revolutions ~~were~~ **R2:C4-aj** are evaluated. **R1:Mi5-a** As the sampling rate is equal to the physical time step of the simulation, the highest resolved frequency (Nyquist frequency) is $46.8\,\mathrm{Hz}$.

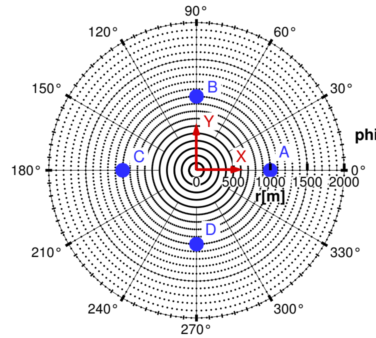

Figure 4. Observer positions for evaluation of aero acoustic emissions. Tower base coordinate system shown in red. View from above, turbine in the center, wind from left.

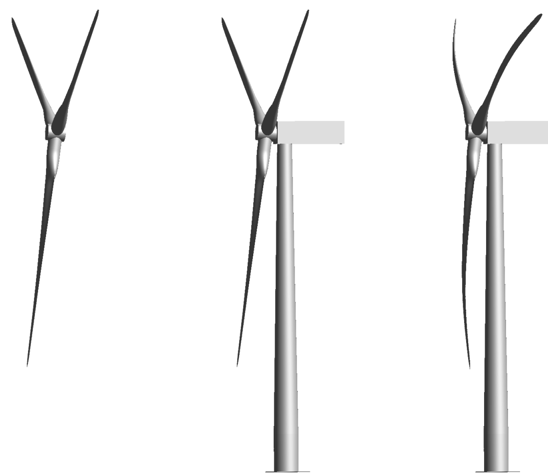

Figure 5. CFD turbine surfaces of cases LC1 (left), LC2 (middle) and LC2_FSC1SD (right). Snapshot with one blade in front of the tower at 180° azimuth.

3 Results

3.1 Rigid simulations

In this section three non-fluid-structure coupled cases are compared at uniform inflow conditions. As reference the rotor only case (LC1) is regarded where unsteady effects on the loads only result from the tilt of the rotor, the proximity to the ground and unsteady flow separation. In a second case, the tower is considered (LC2) and in a third case steady deformation is applied to the blades (LC2_FSC1SD). The CFD surfaces of all three cases are shown in Figure 5.

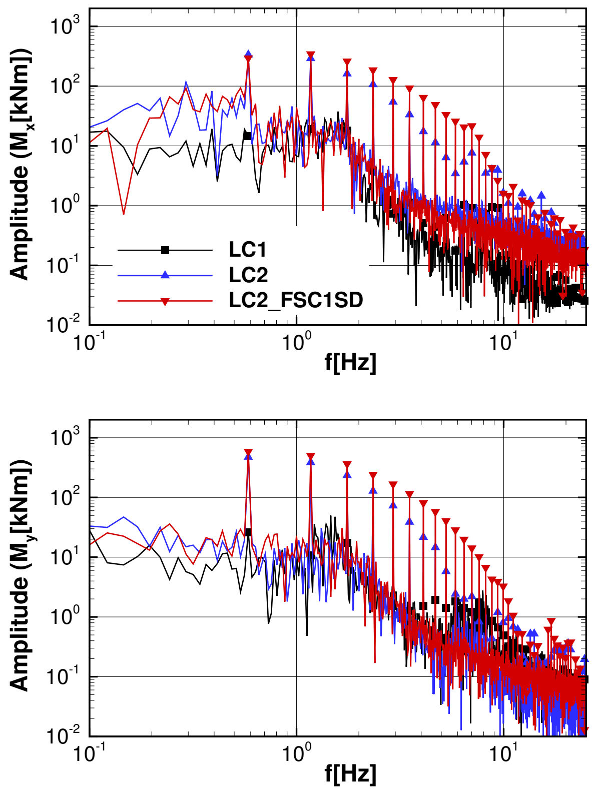

Figure 6. Spectra of ~~tower base loads~~ **R2:AC17-b** aerodynamic loads with respect to tower base (moment reference point) for cases LC1, LC2 and LC2_FSC1SD. **R2:C3-c**

3.1.1 Tower base loads

In the non-fluid-structure coupled cases no unsteady structural forces occur as all structures are rigid. Thus, load fluctuation only arise from aerodynamics. Figure 6 shows the spectra of ~~the aerodynamic loads~~ **R2:C3-d** M_x and M_y of all three cases with respect to the tower base coordinate system **R2:AC17-a** (moment reference point). No distinctive peaks can be found in the spectra of LC1. After including the tower in the simulation (LC2), sharp peaks at the blade-passing frequency and its higher harmonics appear with significantly increased amplitudes up to a frequency of approximately $10\,\mathrm{Hz}$. Regarding ~~F_y and~~ **R2:C3-e** M_x, a general increase of the amplitudes below BPF ~~are~~ **R2:C3-f** is present with a peak at approximately $0.3\,\mathrm{Hz}$ caused by vortex shedding, which will be shown later. In LC2_FSC2SD the distance between tower and blades is reduced due to the steady deformation of the blades. This leads to an increase of the amplitudes at blade-passing harmonics. The relative increase is stronger for higher frequencies. The amplitude of ~~F_x~~ **R2:C3-g** M_y is increased by more than 50% for frequencies between $5\,\mathrm{Hz}$ and $10\,\mathrm{Hz}$. For ~~F_y and~~ **R2:C3-h** M_x the amplitude at BPF stays almost constant while amplitudes are increased for the higher harmonics compared to case LC2. The maximum amplitude of M_x is shifted to the second harmonic of BPF.

The amplitudes of ~~F_z and M_z are much lower compared to the other load components~~ **R2:C3-i** M_z are much lower compared to the other load components and therefore are not shown.

The composition of the **R2:AC18-a** aerodynamic loads was investigated in detail for case LC2_FSC1SD. Therefore, aerodynamic loads on rotor and tower were evaluated separately **R2:AC18-b** with respect to tower base coordinate system (moment reference point). Figure 7 shows the resulting spectra. ~~For all loads except F_z and M_z, the~~ **R2:C3-j** The peak amplitudes of the tower spectra are dominant over the whole frequency range. Especially for ~~F_y and~~ **R2:C3-k** M_x the tower load amplitudes are up to ten times higher compared to the rotor load amplitudes. For ~~F_y and~~ **R2:C3-l** M_x the general level below BPF is higher in the tower load spectra. This can be interpreted as the impact of unsteady flow separation at the tower induced by vortex shedding. This phenomenon, known as von Kármán vortex street, leads to unsteady forces on blunt bodies with a frequency described by the dimensionless Strouhal number. ~~Assuming a Strouhal number of 0.2 and an inflow velocity of $8\,\mathrm{ms}^{-1}$ (reduced due to induction of the rotor), the frequency of the undisturbed vortex shedding should be around $0.32\,\mathrm{Hz}$ with respect to the mean diameter of the tower of $4.9\,\mathrm{m}$.~~ **R2:AC20** Assuming an inflow velocity of $8\,\mathrm{ms}^{-1}$ (reduced due to induction of the rotor) results in a Reynolds number of $2.8 \cdot 10^6$ with respect to the mean diameter of the tower ($4.9\,\mathrm{m}$). The corresponding Strouhal number of approx. 0.24 leads to a theoretical vortex shedding frequency of $0.38\,\mathrm{Hz}$. As both, diameter and inflow velocity are not constant over the length of the tower and inflow is disturbed by the rotor, a broader range of vortex shedding frequencies can be expected ~~. In Figure 10 the time series of aerodynamic loads F_y and M_x acting on the tower are displayed. It is clearly visible that the peaks appearing periodically with the BPF are superimposed with a lower frequency oscillation.~~ **R2:C3-m** **R2:AC21** as it is present in the spectrum of M_x.

~~Figure 10~~ **R2:C3-n**

The surface pressure amplitudes on the tower are displayed in Figure 8 at two different frequencies. At BPF ($0.585\,\mathrm{Hz}$) as well as at $0.292\,\mathrm{Hz}$ where the spectra of ~~F_y and~~ **R2:C3-o** M_x have a local maximum. A strong peak appears at BPF at the front of the tower shifted to the side of the approaching blade. The symmetric shape of the pressure amplitude distribution and the higher amplitudes at the rear side of the tower at $0.292\,\mathrm{Hz}$ can very likely be associated with vortex shedding creating the peak in the load spectra. These observations support the idea of the superposition of blade-passing effects and vortex shedding at the tower.

3.1.2 Aeroacoustic emission

Figure 9 shows the spectra of the SPL for observers ~~A-D for the cases LC1, LC2 and LC2_FSC1SD.~~ **R2:C3-q** C and D for the cases LC1, LC2 and LC2_FSC1SD. The immission at observer A is very similar to the one at observer C. The same applies to observers B and D. The maximum SPL for LC1, the case without tower, occurs at observer B at BPF and is the only prominent peak. The emission at this frequency shows a strong directivity, as the amplitude is much higher at the sides than upstream and downstream of the turbine. The presence of the tower (LC2 and LC2_FSC1SD) causes a massive increase of amplitudes at the BPF harmonics while the broadband noise level stays low. The highest peak appears upstream of the turbine at observer C at the third BPF harmonic and is approx. $4\,\mathrm{dB}$ higher in case LC2_FSC1SD compared to case LC2. The spectra

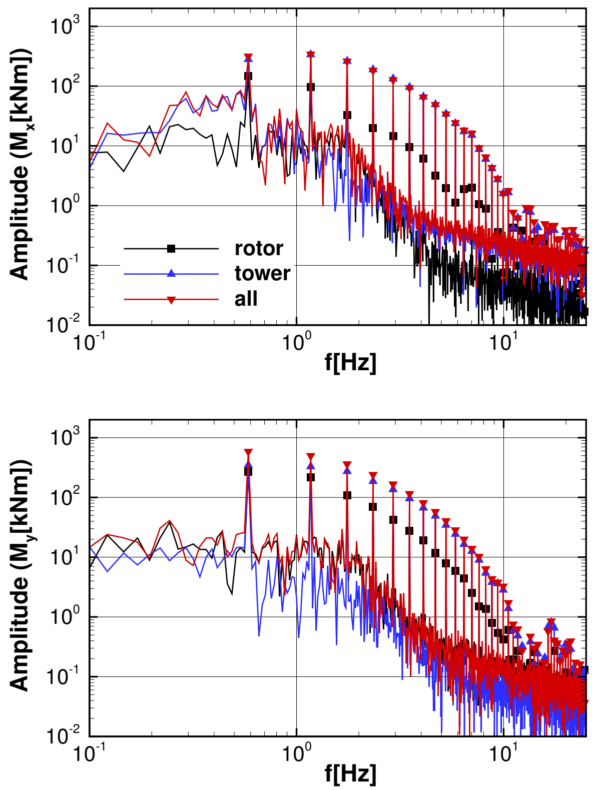

Figure 7. Spectra of ~~tower base loads~~ R2:AC18-c aerodynamic loads with respect to tower base (moment reference point) for case LC2_FSC1SD. Authors Comparison of loads on rotor, tower and all surfaces. R2:C3-p

of case LC2 show only a weak directivity for the BPF harmonics as the amplitudes at the upstream and downstream observers are just slightly lower than at the side observers. A stronger directivity can be observed for case LC2_FSC1SD at BPF where the amplitudes are clearly higher at the upstream and downstream observer. Compared to case LC1 the SPL at frequencies below BPF also rises, but only at observer positions B and D. Comparing LC2_FSC1SD to LC2, the increase of amplitudes due to reduced blade-tower distance is most prominent between fifth and tenth harmonic of BPF where it amounts to more than 10 dB. The SPL peaks drop below 20 dB at around 15 Hz even for case LC2_FSC1SD.

To examine the aeroacoustic noise emission in detail, the noise emission originating from tower and rotor surfaces were evaluated separately for case LC2_FSC1SD. Figure 10 shows the SPL spectra at observer positions ~~A–D~~ R2:C3-t C and D. It can be seen that for all BPF harmonics the calculated SPL emitted by the tower is higher than the one emitted by the rotor. The global maximum of the rotor induced immission is about 8 dB lower compared to the global peak of the tower induced immission, both occur at observer C. The emission from the rotor shows a strong directivity to the upstream and downstream direction, with clearly lower amplitudes at observers B and D. At BPF, the emission of the tower shows the same directivity, yet

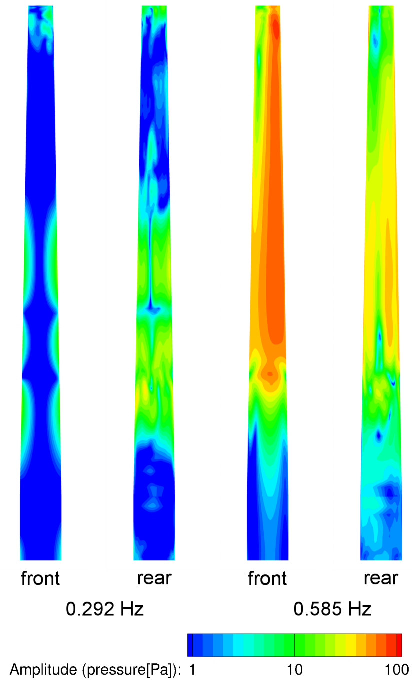

Figure 8. Pressure amplitudes on CFD tower surface of case LC2_FSC1SD at $0.292\,\mathrm{Hz}$ (left) and blade-passing frequency ($0.585\,\mathrm{Hz}$) (right).

less pronounced, whereas the directional differences at higher harmonics of BPF are marginal. The SPL increase in the plane of rotation for frequencies below BPF is mainly caused by the tower emission. This is similar to the increase of amplitudes in the tower base load spectra for ~~F_y and~~ **R2:C3-u** M_x caused by pressure fluctuations on the tower surface which was described in the previous section. Thus SPL increase at frequencies below BPF is very likely induced by surface pressure fluctuations due to vortex shedding at the tower, too. Looking at the noise carpet for the third BPF harmonic in Figure 11 gives more insight into the directivity. The rotor emission is strongly directed towards $20°$ and $190°$, whereas for the tower emission only a small shift of the generally concentric shape towards $220°$ is present. The superposed signal shows a directivity towards $180°/350°$ and is slightly biased upstream. The result also shows that the shape of the SPL isolines beyond approx. $500\,\mathrm{m}$ radius around the turbine is independent of the radius. The same behaviour can be observed for the other harmonics of BPF. Thus, the previously regarded observers at $1000\,\mathrm{m}$ radius are clearly out of near field effects for BPF harmonics.

3.2 Influence of degrees of freedom at uniform inflow

In the second study the cases LC2_FSC1SD, LC2_FSC1 and LC2_FSC3 are regarded. The aim is to evaluate the influence of the degrees of freedom of the structural model on the low-frequency emissions from the wind turbine. Case LC2_FSC1SD has

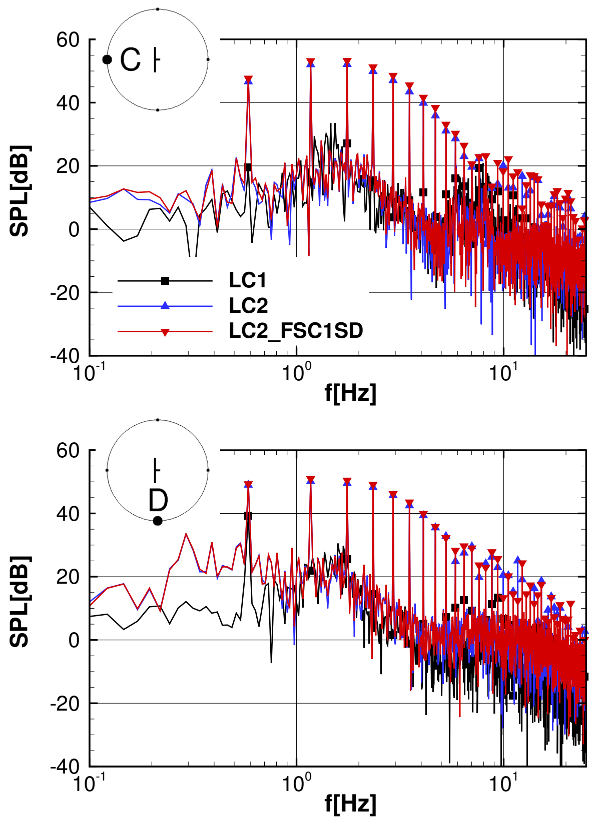

Figure 9. Spectra of unweighted SPL (reference sound pressure of $20\,\mu\mathrm{Pa}$) at ~~4~~ **R2:C3-r** two observer positions on the ground with a distance of $1000\,\mathrm{m}$ to the turbine for cases LC1, LC2 and LC2_FSC1SD. **R2:C3-s**

zero degrees of freedom but considers the mean blade deformation of case LC2_FSC1 where only the rotor blades are flexible, thus it has been chosen as reference case for this study.

3.2.1 Tower base loads

The spectra of the tower base loads for all three cases are plotted in Figure 12. The flexibility of the rotor blades in case LC2_FSC1 has mainly an impact on the amplitudes at harmonics of BPF.~~While the amplitudes in F_x decrease slightly, the amplitudes in F_y rather increase. A clear increase of F_z at BPF and some higher harmonics is present.~~ **R2:C3-w** M_x amplitudes~~also~~ **R2:C3-x** increase with the highest peaks at first and second harmonic of BPF rising by more than 30% compared to case LC2_FSC1SD. On the contrary a decrease is observed for M_y, especially for the second and third harmonic of BPF.~~M_z stays on a much lower level than M_x and M_y but amplitudes at most higher harmonics of BPF are increased compared to the reference case.~~ **R2:C3-y**

There are two effects which go hand in hand both having an influence on the tower base loads. By setting the blades flexible,

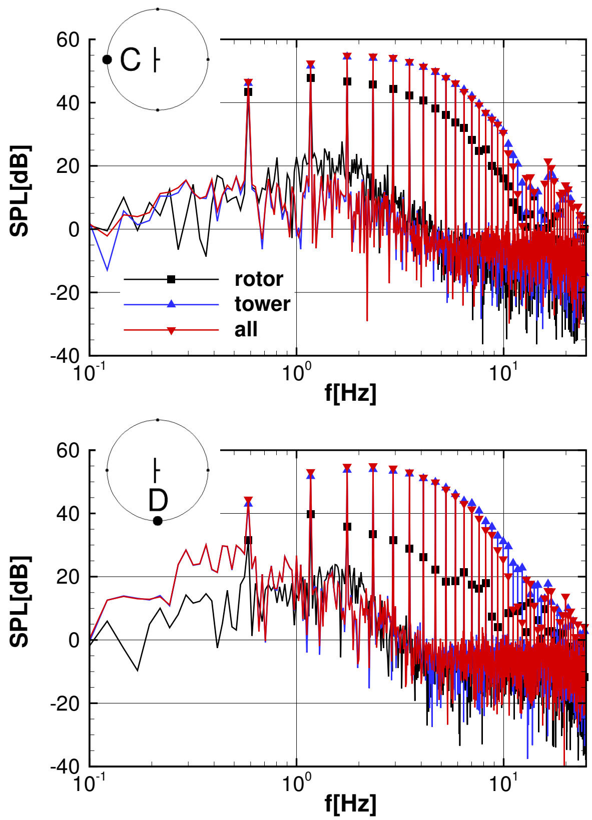

Figure 10. Spectra of unweighted SPL (reference sound pressure of $20\,\mu\mathrm{Pa}$) at ~~4~~ **R2:C3-v** two observer positions on the ground with a distance of $1000\,\mathrm{m}$ to the turbine for case LC2_FSC1SD. Comparison of ~~emission~~ **Authors** noise emitted from rotor, tower and all surfaces.

on the one hand, gravitational forces and inertial forces start acting and on the other hand, aerodynamic forces change due to unsteady deflection of the blades. The mean blade tip deflection applied in case LC2_FSC1SD is $6.34\,\mathrm{m}$ out of plane (OOP) and $-0.58\,\mathrm{m}$ in plane (IP). In case LC2_FSC1 the OOP deflection reaches its maximum of approximately $6.46\,\mathrm{m}$ when the blade is passing the tower, just before the blade deformation is reduced due to the tower blockage. The IP deflection oscillates between $-0.13\,\mathrm{m}$ and $-1.02\,\mathrm{m}$, which is mainly caused by the gravitational force that makes the blade bend downwards. Due to the inertia of the blade, the IP blade tip velocity reaches its maximum just after the tower passage. This increases the absolute velocity of the blade when passing the tower and the relative flow velocity on the blade. On the other hand, the swinging of the blades mainly induces structural forces in y and z direction which explains the increase of ~~F_y and F_z~~ **R2:C3-aa** M_x amplitudes at BPF. The enabled flexibility of the tower in case LC2_FSC3 shows a much stronger impact on the tower base loads compared to case LC2_FSC1 as it significantly changes the structural eigenmodes of the turbine. ~~Regarding the dominant loads F_x, F_y,~~ **R2:C3-ab** In M_x and M_y, the amplitudes at first, second and third harmonics of BPF are clearly reduced. Especially the reduction at BPF is remarkable, over 70% for **R2:C3-ac** both loads ~~all four load components~~. For M_x

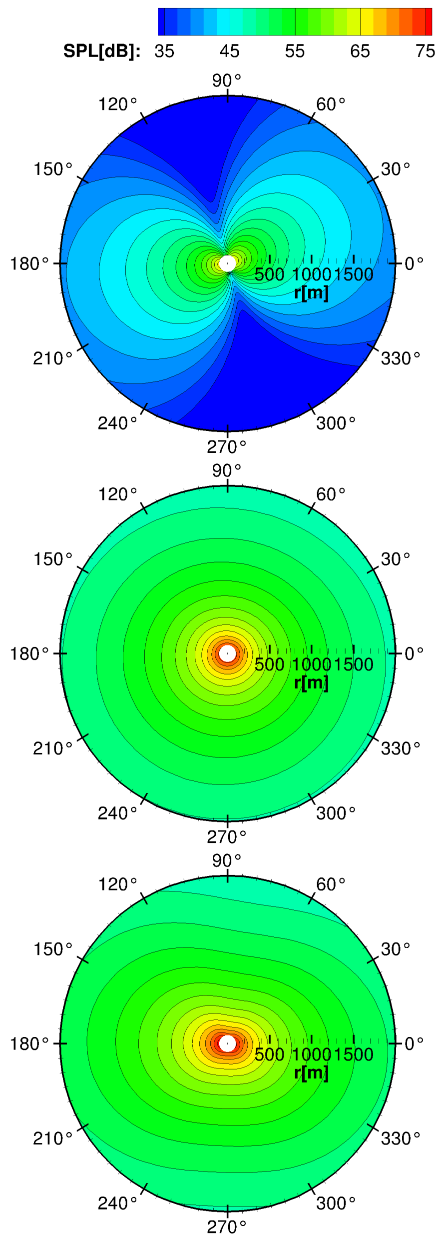

Figure 11. Unweighted SPL (reference sound pressure of $20\,\mu\mathrm{Pa}$) at third BPF harmonic ($1.755\,\mathrm{Hz}$) on ground around the turbine for case LC2_FSC1SD. Aeroacoustic emission from rotor (top), tower (middle) and all surfaces (bottom). ΔSPL between black contour lines is $2\,\mathrm{dB}$.

the amplitude at BPF even drops to the level of the broadband fluctuations of the other two cases. For ~~F_x and~~ **R2:C3-ad** M_y the maximum amplitude shifts to the fifth harmonic of BPF which is close to three structural eigenfrequencies of the turbine. For ~~F_y and~~ **R2:C3-ae** M_x it occurs at approximately $0.32\,\mathrm{Hz}$ which matches with the first side-side bending mode of the

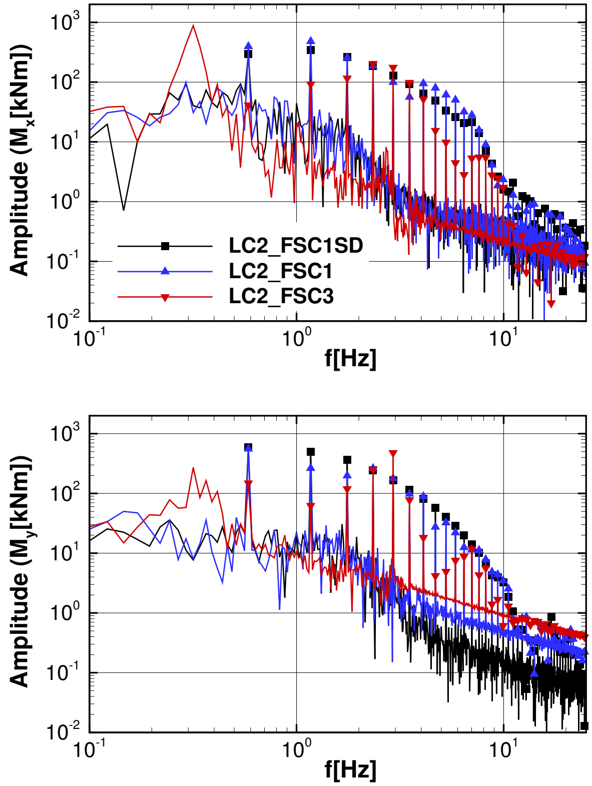

Figure 12. Spectra of ~~tower base loads~~ **R2:C3-z** tower base bending moments for the cases LC2_FSC1SD, LC2_FSC1 and LC2_FSC3.

tower. An increase of the amplitudes in the frequency range around 0.32 Hz can also be observed for~~F_x and~~ **R2:C3-af** M_y, yet less pronounced. The first fore-aft bending mode is also at this frequency but the aerodynamic damping is much higher compared to the side-side direction.~~For F_z amplitudes at higher harmonics of BPF are increased but the maximum amplitude, occurring at BPF, is reduced. For M_z a further increase of the amplitudes of second to sixth harmonics of BPF is present and the maximum amplitude is increased and shifted to the fifth harmonic of BPF.~~ **R2:C3-ag**

3.2.2 Aeroacoustic emission

The increase of degrees of freedom in the structural model only marginally influences the SPL at the ~~observer positions A-D (). The spectra at observer positions A and C show a small decrease of the amplitude at BPF while there is a small increase at second to sixth harmonics of BPF. However, observers B and D show a small increase at BPF while amplitudes of higher harmonics are almost unchanged.~~ **R2:C3-ah** observers. The spectrum at observer position C shows a small decrease of the amplitude at BPF while there is a small increase at second to sixth harmonics of BPF. However, observer D shows a small increase at BPF while amplitudes of higher harmonics are almost unchanged. Generally, the effect is a bit stronger for case LC2_FSC3. These small changes might be an impact of the slightly reduced blade-tower distance and the increased blade tip velocity when the blade passes the tower which was reported in the previous section. For frequencies below BPF, the maximum amplitude increases slightly which could be induced by the structural eigenmodes of the turbine as well as by the impact of vortex shedding at the tower.

~~Figure 16: Spectra of unweighted SPL (reference sound pressure of 20 μPa) at 4 observer positions on the ground with a distance of 1000 m to the turbine for cases LC2_FSC1SD, LC2_FSC1 and LC2_FSC3.~~ **R2:C3-aj**

3.3 Influence of inflow

In the last study the influence of inflow conditions on the tower base loads and on the aeroacoustic emission is investigated. While uniform inflow was applied for the previous studies, more realistic inflow is considered in this study. Two cases, one with vertically sheared inflow (LC3_FSC3) and one with turbulent vertically sheared inflow (LC4_FSC3) are compared to the uniform inflow case (LC2_FSC3). For the turbulent inflow case a longer time series is evaluated in order to obtain more representative results.

3.3.1 Tower base loads

The spectra of tower base loads in Figure 13 show that for case LC3_FSC3 an increase of amplitudes is only present for ~~F_x, F_z, M_y and M_z and only~~ **R2:C3-ak** M_y at BPF.~~Especially the amplitude of M_z at BPF rises to a remarkably high level.~~ **R2:C3-al** Amplitudes at higher harmonics of BPF tend to reduce for~~all loads except for M_z~~ **R2:C3-am** M_x and M_y. The result also shows that the broadband load level at frequencies between first and fifth BPF harmonics rises. For~~F_y and~~ **R2:C3-an** M_x there is a clear peak just above 1 Hz which even exceeds the peak at BPF **R2:C3-ao** ~~for M_x~~. The reduction of amplitudes at higher harmonics of BPF can be explained as a result of the reduced inflow velocity below hub height due to the power law profile. Because of the lower aerodynamic thrust in this region, OOP deflection in front of the tower reduces to approximately $5.5\,\mathrm{m}$ compared to $6.46\,\mathrm{m}$ in case LC2_FSC3. The rise of amplitudes at BPF can be explained as an effect of vertical shear. While blade-passing is a short pulse and many higher harmonics of BPF are excited, the effect of vertical shear stretches over the whole revolution and is much closer to a sine function. Thus, the excitation of higher harmonics of BPF is much weaker compared to blade-passing. The combination of vertical shear and reduced blade-passing effect finally leads to an increase of amplitudes at BPF while amplitudes at higher harmonics decrease.

By superimposing turbulence to the vertically sheared flow in case LC4_FSC3, the character of the spectra changes as the amplitudes at BPF harmonics become much less prominent. There are some clear peaks remaining, but the broadband load level massively increases. The global maximum now arises for M_y at approximately $0.32\,\mathrm{Hz}$ corresponding to an eigenmode of the structural model. Additionally the amplitude at BPF is strongly increased for~~F_x, F_y,~~ **R2:C3-aq** M_x and M_y; however, side peaks occur that are partially even higher. The amplitude at approximately $1\,\mathrm{Hz}$ further increases compared to case LC3_FSC3 and another wide peak appears at frequencies around approximately $2.75\,\mathrm{Hz}$, which again corresponds to nearby structural eigenmodes. The higher amplitudes at frequencies near to structural eigenmodes can be explained by the broadband excitation

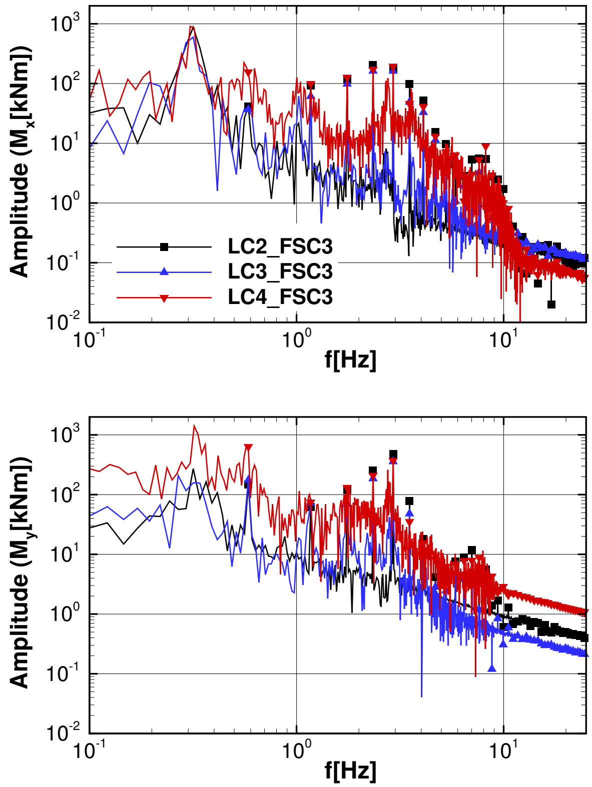

Figure 13. Spectra of ~~tower base loads~~ **R2:C3-ap** tower base bending moments for the cases LC2_FSC3, LC3_FSC3 and LC4_FSC3.

due to the influence of turbulent inflow on the aerodynamic loads. Without turbulent inflow the main excitation occurs at BPF harmonics because all unsteady effects except for the vortex shedding are periodic with BPF (blade-tower interaction, tilt angle, vertical shear).

3.3.2 Aeroacoustic emissions

Figure 14 shows the spectra of the acoustic immission at observers ~~A to D~~ **R2:C3-ar** C and D for the regarded cases. The vertically sheared inflow (case LC3_FSC3) leads to a slight decrease of SPL at BPF harmonics with a stronger effect at higher frequencies. Only a small increase of amplitude can be observed at BPF for observer~~s B and~~ **R2:C3-as** D. For observer~~s~~ ~~A and~~ **R2:C3-at** C an increase in the broadband noise level between approximately 2 Hz and 10 Hz can be found, but it does not exceed 30 dB. The reduction of SPL can be explained with the reduced blade tip deflection in front of the tower already mentioned above, which reduces the pressure fluctuations on the tower. Taking the turbulent inflow into account (case LC4_FSC3) leads to an increase of the broadband noise level due to turbulent inflow noise, generated by the interaction of the rotor blade with the turbulence. The inflow noise is emitted from the rotor and predominantly directed in upstream and

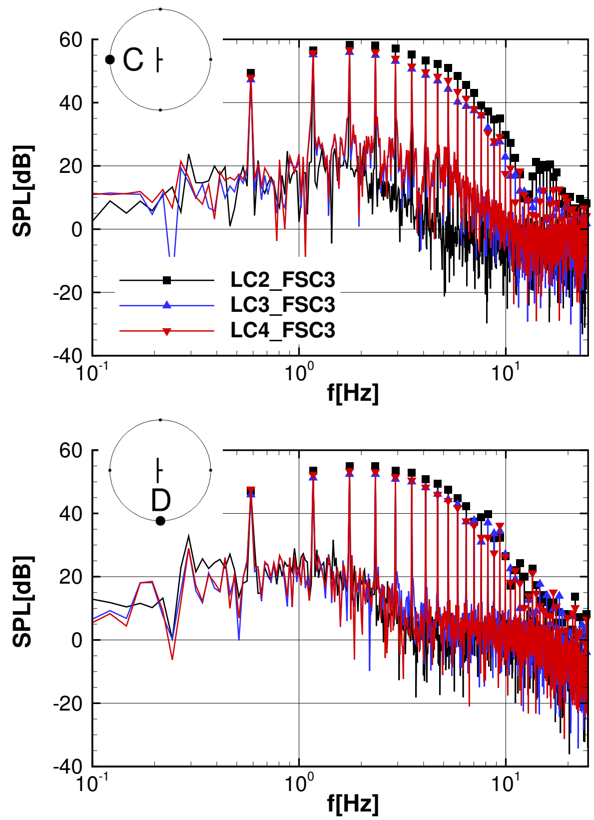

Figure 14. Spectra of unweighted SPL (reference sound pressure of $20\,\mu\mathrm{Pa}$) at ~~4~~ **R2:C3-ap** two observer positions on the ground with a distance of $1000\,\mathrm{m}$ to the turbine for cases LC2_FSC3, LC3_FSC3 and LC4_FSC3.

downstream direction, leading to higher broadband noise levels at observer~~s A and~~ **R2:C3-au** C compared to observer~~s B and~~ **R2:C3-av** D. Since the rotor blades encounter the turbulence at considerably higher relative velocity than the tower, the emission from the tower hardly increases compared to case LC3_FSC3. However, despite the increased broadband noise level, the peaks at BPF harmonics are still dominant at all four observer positions.

4 Discussion

In the first study the influence of the presence of the tower and of steady blade deformation on low-frequency emissions was evaluated at uniform inflow conditions in standalone CFD simulations. Concerning the aerodynamic loads, the presence of the tower leads to an increase of amplitudes at BPF and its higher harmonics. Applying a steady deformation to the rotor blades further increases the amplitudes especially for higher harmonics due to the stronger blade-tower interaction. Splitting the loads up into rotor and tower loads shows that the major part of the fluctuations originates from the tower and is caused by blade-tower interaction. Load oscillations induced by vortex shedding can be observed but do not play an important role.

Evaluating the aeroacoustic immission on the ground at a distance of $1000\,\mathrm{m}$ shows similar results. Through the presence of the tower a tonal noise emission with prominent peaks at BPF harmonics arises. Reduced blade-tower distance further increases the amplitudes of BPF harmonics especially at higher frequencies. Comparing the contributions of tower and rotor to the noise emission shows a strong directivity for the rotor emission in the direction of the rotor axis and a weak directivity for the tower emission except at BPF. Generally the emission from the tower is stronger in all directions in the regarded frequency range. This corresponds to the findings by Yauwenas et al. (2017) who did research on blade-passage noise and claimed a significant contribution of the tower. While Yauwenas et al. investigated a small model turbine with a symmetric blade in stationary air and a BPF of $45\,\mathrm{Hz}$, the present study shows that their assumption is also valid for a realistic multi megawatt turbine under uniform inflow and a BPF in the low frequency range.

In a second study, the influence of degrees of freedom in the structural model was investigated using three cases, one with steady blade deformation already regarded in the first study, another with flexible blades and a third with additionally flexible tower and foundation. Flexible blades have only a minor impact on the calculated tower base loads. Structural eigenmodes play a more significant role in the third case when tower and foundation are flexible too. The peaks at BPF harmonics are still prominent but the amplitudes change and the maxima are shifted towards BPF harmonics close to structural eigenfrequencies. Additionally, peaks corresponding to the first bending modes of the tower ($0.32\,\mathrm{Hz}$) occur, being dominant in ~~F_y and M_x spectra~~ **R2:C3-aw** the spectrum of M_x. Concerning aeroacoustics, the emission slightly increases but no clear influence of structural eigenmodes can be found in the regarded frequency range.

The third study deals with the influence of the inflow condition on the emissions. Uniform inflow is compared to vertically sheared inflow with and without turbulence. For vertical shear inflow tower base loads tend to increase at BPF and decrease at higher harmonics of BPF. With superimposed turbulence the peaks become much less prominent since the broadband load level rises. Amplitudes at frequencies close to structural eigenmodes rise and BPF harmonics become less dominant in the spectra. The tonal noise level of the aeroacoustic emission tends to reduce slightly with the vertical shear and increase again due to the superimposed turbulence. The broadband noise level strongly increases especially for observers upstream and downstream of the turbine, which is mainly caused by turbulent inflow noise emitted by the rotor. Thus, the BPF harmonics become less prominent but are still dominant in the spectra.

As a generic wind turbine was investigated, no measurements for validation are available. Nevertheless, a qualitative comparison between the presented results and two studies found in literature is drawn. Zieger and Ritter (2018) showed seismic measurements in Germany that suggest an independence of discrete frequency peaks and blade-passing frequency. Although the amplitudes increase with increasing wind speed and rotational speed respectively, the frequencies of the peaks do not change. This can be interpreted as a dominance of structural eigenmodes of the turbine in the origin of the seismic waves. However, at high (rated) rotational speed the dominant frequencies correspond very well to harmonics of the blade-passing frequency. Saccorotti et al. (2011) analyzed seismic measurements of a gravitational wave observatory in Italy close to a wind farm and found steady spectral lines as well as time-varying peaks which could all be identified as emitted by a wind turbine. The results of both studies coincide with the findings of the presented paper where tower base loads at BPF harmonics close to eigenfrequencies of the turbine are prominent in the spectra. The tonal character of the low-frequency noise was also shown in acoustic field measurements (Hansen et al., 2017; Pilger and Ceranna, 2017). They showed that the BPF harmonics are dominant in the measured spectra and thus the peak frequencies shift depending on the rotational speed of the turbine. Pilger and Ceranna furthermore compared measurements of a single 200 kW turbine to estimated SPL from the Viterna method (Viterna, 1981). They found an underestimation of SPL which they explained with environmental conditions neglected in the model. Taking the present study into account it is more likely that the neglect of tower emission in the Viterna method has a major impact on the results.

Despite the advanced modelling approach applied in the presented study, there are still several limitations that have to be mentioned. In the applied FW-H calculations effects of unsteady flow field, refraction and reflection of acoustic waves and atmospheric layering are not taken into account for the propagation. On the other hand, this makes the method very suitable for the investigation of the aeroacoustic emission of the turbine, as the immission at the observer positions is not influenced by the effects mentioned above. Due to the computationally expensive CFD approach, there are limitations concerning the length of the time series and temporal resolution and consequently the statistical convergence of the results and the resolved frequency range. Although the flexibility of rotor blade, tower and foundation was considered in the simulations further deegrees of freedom were neglected. The drive train was kept totally rigid and at fixed rotational speed. As *SIMPACK* is a multibody solver and only deformations of points along a beam are transferred, eigenmodes of the shell cannot be considered in the presented approach. However, the mentioned shortcomings do not not change general findings of this paper.

5 Conclusions

In the present paper the low-frequency emissions from a generic 5 MW turbine were investigated using a high fidelity time resolved fluid-structure coupled CFD approach. Three different studies were conducted to identify sources, to better understand mechanisms and to evaluate the influence of the model complexity on the resulting emissions. Tower base loads are compared to study the effect of structure-borne noise as seismic wave propagation cannot be calculated with the presented method. The aeroacoustic noise propagation is computed using a Ffowcs-Williams Hawkings method. To consider aeroelasticity in the simulations a new coupling of the CFD solver *FLOWer* to the MBS solver *SIMPACK* was developed and is presented in this paper. With this method not only blade deformation can be taken into account, but deformations, translations and rotations of all parts of the turbine. Thus, fluid-structure coupled simulations with flexible tower and foundation could be conducted.
~~As a high fidelity approach is used, the aerodynamic results are of high quality.~~ **R2:AC23** A major advantage compared to lower fidelity approaches is that, as all geometries of the turbine are fully resolved, the unsteady pressure distributions on all surfaces, and thus all aerodynamic loads, are a direct outcome of the simulations. Regarding the aeroacoustic emission it was found that the blade-tower interaction plays a key role and the noise emitted from the tower is higher compared to the noise emitted from the rotor. Only an indirect impact of fluid-structure-coupling on the aeroacoustics could be observed. Elastic blades reduce the distance between blade and tower and thus increase the strength of the blade-tower interaction. Turbulent inflow on the other side mainly influences the broadband noise level of the rotor. For the regarded turbulence level of 16% the noise has a tonal character with dominant peaks at blade-passing frequency harmonics.

Blade-tower interaction also has a great influence on the tower base loads; however, with increasing degrees of freedom structural eigenmodes play a much stronger role than for the aeroacoustic emission and amplitudes at eigenfrequencies become more dominant when turbulent inflow is applied. Nevertheless, blade-passing frequency harmonics can still be identified in the spectra. For aerodynamic load fluctuations at uniform inflow it was found that the contribution of the tower exceeds the contribution of the rotor.

Several conclusions for the modelling of low-frequency emissions using CFD simulations can be drawn from the conducted studies. The blade-tower interaction was found to be the main source of aeroacoustic noise and triggers a major part of the aerodynamic load fluctuations. The tower itself as well as a realistic blade-tower distance has to be considered in the simulation to capture the blade-tower interaction properly. Fluid-structure coupling is the most appropriate way to a realistic blade-tower distance and is mandatory if structural emission shall be regarded. Moreover the acoustic emission from the tower has to be considered in the noise evaluation and the loads on the tower have to be included in the fluid-structure coupling. Concerning the structural emission, not only the flexibility of the rotor blades but also of tower and foundation have to be taken into account as they change the character of the tower base load spectra. Turbulent inflow should also be taken into account, because it enhances the excitation of structural eigenmodes.

The findings can be transferred to any modelling method of low-frequency emissions from wind turbines. The method has to be capable of capturing the impact of blade-passing not only on the blades but also on the tower and its effect on the one hand on the aerodynamic load fluctuations and on the other hand on the aeroacoustic noise emission.

Future work will deal with several of the listed limitations. A slightly smaller commercial wind turbine will be investigated numerically with the presented approach and field measurements will be available for comparison. Subsequently, the turbine will be simulated taking into account the operational conditions of the measurements. The influence of full shell coupling on the low-frequency emission will be investigated in a future study. Based on the presented findings, constructional measures as lattice towers, increased blade tower distance or swept blades are likely to reduce low-frequency emissions and should be taken into account for future research.

Data availability. Data of the NREL $5\,\mathrm{MW}$ turbine is available from Jonkman et al. (2009).

Competing interests. The authors declare that they have no conflict of interest.

Acknowledgements. The studies ~~where~~ **Authors** were conducted as part of the joint research project "Objective Criteria for Seismic and Acoustic Emission of Inland Wind Turbines (TremAc), FKZ 0325839A", funded by the German Federal Ministry for Economic Affairs and

Energy (BMWi). The authors are grateful for the financial support. The authors gratefully acknowledge the *High Performance Computing Center Stuttgart* for providing computational resources within the project *WEALoads*.

References

Arnold, M., Cheng, P. W., Biskup, F., et al.: Simulation of Fluid-Structure-Interaction on Tidal Current Turbines Based on Coupled Multibody and CFD Methods, in: The Twenty-third International Offshore and Polar Engineering Conference, International Society of Offshore and Polar Engineers, 2013.

Bekiropoulos, D., Lutz, T., Baltazar, J., Lehmkuhl, O., and Glodic, N.: D2013-3.1: Comparison of benchmark results from CFD-Simulation, Deliverable report, KIC-OFFWINDTECH, 2013.

Bozorgi, A., Ghorbaniasl, G., and Nourbakhsh, S.: The reduction in low-frequency noise of horizontal-axis wind turbines by adjusting blade cone angle, International Journal of Environmental Science and Technology, pp. 1–14, 2018.

Ghasemian, M. and Nejat, A.: Aerodynamic noise prediction of a horizontal Axis wind turbine using improved delayed detached eddy simulation and acoustic analogy, Energy Conversion and Management, 99, 210–220, 2015.

Gortsas, T. V., Triantafyllidis, T., Chrisopoulos, S., and Polyzos, D.: Numerical modelling of micro-seismic and infrasound noise radiated by a wind turbine, Soil Dynamics and Earthquake Engineering, 99, 108–123, 2017.

Hansen, K. L., Zajamšek, B., and Hansen, C. H.: The Occurrence of Nocturnal Wind Farm Rumbling Noise, 7th International Conference on Wind Turbine Noise Rotterdam, pp. 1–11, 2017.

Illg, J., Lutz, T., and Krämer, E.: Aeroacoustic Simulation of an Airfoil in Turbulent Inflow, in: 6th International Conference on Wind Turbine Noise, Glasgow, 2015.

Jassmann, U., Berroth, J., Matzke, D., Schelenz, R., Reiter, M., Jacobs, G., and Abel, D.: Model predictive control of a wind turbine modelled in Simpack, in: Journal of Physics: Conference Series, vol. 524, IOP Publishing, 2014.

Jonkman, J., Butterfield, S., Musial, W., and Scott, G.: Definition of a 5-MW reference wind turbine for offshore system development, Tech. rep., National Renewable Energy Lab.(NREL), Golden, CO (United States), 2009.

Knopper, L. D., Ollson, C. A., McCallum, L. C., Whitfield Aslund, M. L., Berger, R. G., Souweine, K., and McDaniel, M.: Wind turbines and human health, Frontiers in public health, 2, 63, 2014.

Kowarsch, U., Keßler, M., and Krämer, E.: High order CFD-simulation of the rotor-fuselage interaction, in: 39th European Rotorcraft Forum, Moscow, 2013.

Kranzinger, P. P., Kowarsch, U., Schuff, M., Keßler, M., and Krämer, E.: Advances in parallelization and high-fidelity simulation of helicopter phenomena, in: High Performance Computing in Science and Engineering´ 15, pp. 479–494, Springer, 2016.

Kroll, N., Rossow, C.-C., Becker, K., and Thiele, F.: The MEGAFLOW project, Aerospace Science and Technology, 4, 223–237, 2000.

Li, Y., Castro, A., Martin, J., Sinokrot, T., Prescott, W., and Carrica, P.: Coupled computational fluid dynamics/multibody dynamics method for wind turbine aero-servo-elastic simulation including drivetrain dynamics, Renewable Energy, 101, 1037–1051, 2017.

Liu, W.: A review on wind turbine noise mechanism and de-noising techniques, Renewable Energy, 108, 311–320, 2017.

Luhmann, B., Seyedin, H., and Cheng, P.-W.: Aero-structural dynamics of a flexible hub connection for load reduction on two-bladed wind turbines, Wind Energy, 20, 521–535, 2017.

Lutz, T., Arnold, B., Bekiropoulos, D., Illg, J., Krämer, E., Wolf, A., Hann, R., and Kamruzzaman, M.: Prediction of Flow-Induced Noise Sources of Wind Turbines and Application Examples, International Journal of Aeroacoustics, 2015.

Madsen, H. A.: Low frequency noise from wind turbines mechanisms of generation and its modelling, Journal of Low Frequency Noise, Vibration and Active Control, 29, 239–251, 2010.

Mann, J.: The spatial structure of neutral atmospheric surface-layer turbulence, Journal of fluid mechanics, 273, 141–168, 1994.

Matha, D., Hauptmann, S., Hecquet, T., and Kühn, M.: Methodology and results of loads analysis of wind turbines with advanced aeroelastic multi-body simulation, DEWEK, Bremen, 2010.

Menter, F. R.: Two-equation eddy-viscosity turbulence models for engineering applications, AIAA journal, 32, 1598–1605, 1994.

Pilger, C. and Ceranna, L.: The influence of periodic wind turbine noise on infrasound array measurements, Journal of Sound and Vibration, 388, 188–200, 2017.

Saccorotti, G., Piccinini, D., Cauchie, L., and Fiori, I.: Seismic noise by wind farms: a case study from the Virgo Gravitational Wave Observatory, Italy, Bulletin of the Seismological Society of America, 101, 568–578, 2011.

Sayed, M., Lutz, T., and Krämer, E.: Aerodynamic investigation of flow over a multi-megawatt slender bladed horizontal-axis wind turbine, Renewable Energies Offshore, 2015.

Sayed, M., Lutz, T., Krämer, E., Shayegan, S., Ghantasala, A., Wüchner, R., and Bletzinger, K.-U.: High fidelity CFD-CSD aeroelastic analysis of slender bladed horizontal-axis wind turbine, in: Journal of Physics: Conference Series, vol. 753, IOP Publishing, 2016.

Schepers, J., Ceyhan, O., Boorsma, K., Gonzalez, A., Munduate, X., Pires, O., Sørensen, N., Ferreira, C., Sieros, G., Madsen, J., Voutsinas, S., Lutz, T., Barakos, G., Colonia, S., Heißelmann, H., Meng, F., and Croce, A.: Latest results from the EU project AVATAR: Aerodynamic modelling of 10 MW wind turbines, in: Journal of Physics: Conference Series, vol. 753, IOP Publishing, 2016.

Schuff, M., Kranzinger, P., Keßler, M., and Krämer, E.: Advanced CFD-CSD coupling: Generalized, high performant, radial basis function based volume mesh deformation algorithm for structured, unstructured and overlapping meshes, in: Proceedings of the 40th European Rotorcraft Forum. Southhampton. Great Britain, 2014.

Schulz, C., Klein, L., Weihing, P., and Lutz, T.: Investigations into the interaction of a wind turbine with atmospheric turbulence in complex terrain, in: Journal of Physics: Conference Series, vol. 753, p. 032016, IOP Publishing, 2016a.

Schulz, C., Meister, K., Lutz, T., and Krämer, E.: Investigations on the wake development of the MEXICO rotor considering different inflow conditions, in: New Results in Numerical and Experimental Fluid Mechanics X, pp. 871–882, Springer, 2016b.

Stammler, K. and Ceranna, L.: Influence of wind turbines on seismic records of the Gräfenberg array, Seismological Research Letters, 87, 1075–1081, 2016.

Streiner, S., Hauptmann, S., Kühn, M., and Krämer, E.: Coupled fluid-structure simulations of a wind turbine rotor, in: Deutsche Windenergie-Konferenz (DEWEK). Bremen, Germany: DEWI-German Wind Energy Institute, 2008.

Styles, P., Stimpson, I., Toon, S., England, R., and Wright, M.: Microseismic and infrasound monitoring of low frequency noise and vibrations from windfarms, Recommendations on the Siting of Windfarms in the Vicinity of Eskdalemuir, Scotland, Report to MOD/FTI/BWEA, 125pp, 2005.

Turnbull, C., Turner, J., and Walsh, D.: Measurement and level of infrasound from wind farms and other sources, Acoustics Australia, 40, 45–50, 2012.

Van den Berg, G.: The beat is getting stronger: the effect of atmospheric stability on low frequency modulated sound of wind turbines, Journal of Low Frequency Noise, Vibration and Active Control, 24, 1–23, 2005.

Viterna, L. A.: The NASA-LERC wind turbine noise prediction code, NASA CP, 2185, 1981.

Weihing, P., Letzgus, J., Bangga, G., Lutz, T., and Krämer, E.: Hybrid RANS/LES capabilities of the flow solver FLOWer-application to flow around wind turbines, in: The 6th Symposium on Hybrid RANS-LES Methods, Strassbourg, 2016.

Yauwenas, Y., Zajamšek, B., Reizes, J., Timchenko, V., and Doolan, C. J.: Numerical simulation of blade-passage noise, The Journal of the Acoustical Society of America, 142, 1575–1586, 2017.

Zajamšek, B., Hansen, K. L., Doolan, C. J., and Hansen, C. H.: Characterisation of wind farm infrasound and low-frequency noise, Journal of Sound and Vibration, 370, 176–190, 2016.

Zieger, T. and Ritter, J. R.: Influence of wind turbines on seismic stations in the upper rhine graben, SW Germany, Journal of Seismology, 22, 105–122, 2018.